1-1-2011

Modeled and observed N-2 Lyman-Birge-Hopfield band emissions: A comparison

R. W. Eastes
University of Central Florida

D. J. Murray
University of Central Florida

A. Aksnes

S. A. Budzien

R. E. Daniell

See next page for additional authors

Modeled and observed N_2 Lyman-Birge-Hopfield band emissions: A comparison

R. W. Eastes,[1,2] D. J. Murray,[2] A. Aksnes,[1,3] S. A. Budzien,[4] R. E. Daniell,[5] and A. Krywonos[1]

Received 30 December 2010; revised 12 September 2011; accepted 14 September 2011; published 7 December 2011.

[1] A thorough understanding of how the N_2 Lyman-Birge-Hopfield (LBH) band emissions vary with altitude is essential to the use of this emission by space-based remote sensors. In this paper, model-to-model comparisons are first performed to elucidate the influence of the solar irradiance spectrum, intrasystem cascade excitation, and O_2 photoabsorption on the limb profile. Next, the observed LBH emissions measured by the High resolution Ionospheric and Thermospheric Spectrograph aboard the Advanced Research and Global Observation Satellite are compared with modeled LBH limb profiles to determine which combination of parameters provides the best agreement. The analysis concentrates on the altitude dependence of the LBH (1,1) band, the brightest LBH emission in the observations. In the analysis, satellite drag data are used to constrain the neutral densities used for the data-to-model comparisons. For the average limb profiles on two of the three days analyzed (28, 29, and 30 July 2001), calculations using direct excitation alone give slightly better agreement with the observations than did calculations with cascading between the singlet electronic N_2 states ($a^1\Pi_g$, $a'\Sigma^-_u$, and $w^1\Delta_u$); however, the differences between the observed profiles and either model are possibly greater than the differences between the models. Nevertheless, both models give excellent agreement with the observations, indicating that current models provide an adequate description of the altitude variation of the N_2 LBH (1,1) band emissions. Consequently, when using the LBH bands to remotely sense thermospheric temperatures, which can be used to provide an unprecedented view of the thermosphere, the temperatures derived have a negligible dependence on the model used.

Citation: Eastes, R. W., D. J. Murray, A. Aksnes, S. A. Budzien, R. E. Daniell, and A. Krywonos (2011), Modeled and observed N_2 Lyman-Birge-Hopfield band emissions: A comparison, *J. Geophys. Res.*, *116*, A12308, doi:10.1029/2010JA016417.

1. Introduction

[2] Far ultraviolet (FUV) remote sensing of the Earth's thermosphere has provided valuable insights into the solar and magnetospheric forcing of our space environment [e.g., *Meier*, 1991]. One of the most important FUV emissions is the N_2 Lyman-Birge-Hopfield (LBH) bands (~1270 to 2800 Å). These bands have been used on several satellite missions, e.g., the Ultraviolet Imager (UVI) on Polar [*Torr et al.*, 1995] and the Global Ultraviolet Imager (GUVI) on the Thermosphere Ionosphere Mesosphere Energetics and Dynamics (TIMED) satellite [*Christensen et al.*, 2003; *Meier et al.*, 2005; *Strickland et al.*, 2004; *Zhang et al.*, 2004]. Future missions will also use these bands. Recent work [*Eastes et al.*, 2008] shows that, using the LBH bands, thermospheric temperatures could, for the first time, be continuously monitored with sufficient precision to observe tides and waves across the entire dayside. In order for the LBH bands to be used reliably, an accurate understanding of the emission is essential. However, there are two mechanisms, cascade from other singlet states and direct excitation from the N_2 ground state, for the LBH bands. The effects of cascade, about which our knowledge is limited, on the altitudinal variation of the emission needs to be clarified since the shape alone is sometimes used, and the interpretation of the total brightness may depend on the shape of the profile. Variations in the solar spectrum and the amount of O_2 photoabsorption also affect the altitude profile. This paper examines the effects of all three factors on the agreement between the observed variations in emission with altitude and those calculated. While differences between the peak altitude of the actual emission profile and that modeled are inconsequential for some uses of N_2 LBH band observations, a 5 km difference would change, by 30–50 K, the temperature attributed to the atmosphere at the (modeled) peak altitude.

[1]Florida Space Institute, Kennedy Space Center, Florida, USA.
[2]Department of Physics, University of Central Florida, Orlando, Florida, USA.
[3]Now at Faculty of Mathematics and Natural Sciences, University of Bergen, Bergen, Norway.
[4]Naval Research Laboratory, Washington, DC, USA.
[5]Ionospheric Physics Consulting, Stoughton, Massachusetts, USA.

0148-0227/11/2010JA016417

Such a difference can be significant in comparison to the statistical uncertainties for rotational temperatures from LBH band observations. Fortunately, the results indicate that any differences are likely to be substantially smaller (~1 km).

[3] Although the exospheric temperature, which also affects the profile and is considered in the analysis, the densities, and consequently the temperatures, are normalized to satellite drag measurements, eliminating most of the uncertainty in the exospheric temperatures and simplifying comparison of the other factors influencing altitude profiles of the LBH bands. Also not considered is the shape of the direct excitation cross sections, although recent measurements differ significantly in shape from earlier ones.

[4] The first of the factors examined is the effect of excitation by cascade within the singlet states of N_2, the source of the LBH emission. Modeled LBH brightness (i.e., column emission rate) from first principles airglow models, such as the Atmospheric Ultraviolet Radiance Integrated Code (AURIC) [*Strickland et al.*, 1999] and the Continuous Slowing Down (CSD) model [*Jasperse*, 1976], assume direct excitation of the N_2 ($a^1\Pi_g$) state from the ground state. However, *Cartwright* [1978] suggested intrasystem cascading could significantly increase the emissions from the LBH bands. A possible indicator of a cascade contribution, enhanced populations of the lower vibrational levels, relative to direct excitation, were later reported by *Eastes et al.* [1985] and by *Eastes and Sharp* [1987]. *Budzien et al.* [1994] reported a similar enhancement in observations from the Ultra-Violet Limb Imaging experiment aboard Space Transport System number 39 (STS-39). They found, in observations from above 200 km, significant differences from electron impact excitation of N_2 in the distribution of the vibrational populations, even when including excitation from $v > 0$ of the ground state. In addition *Budzien et al.* [1994] found that their modeled brightnesses, which did not include cascade, were low by a factor of 1.4–1.6.

[5] By including radiative and collisional cascading between the three lowest singlet states of N_2 ($a^1\Pi_g$, $a'^1\Sigma^-_u$, and $w^1\Delta_u$), *Eastes* [2000] was able to provide good agreement between the relative distribution of modeled and observed vibrational populations. Furthermore, *Eastes* [2000] found that the inclusion of cascading increased the total emission from the LBH bands by a factor of ~1.6, consistent with the results of *Budzien et al.* [1994].

[6] The second of the factors examined is the influence of the Sun's soft X-ray and extreme ultraviolet (EUV) spectrum, the energy source for producing the LBH emission during the day. Since the shorter solar wavelengths deposit their energy lower in the atmosphere, changes in the shape of the solar spectrum can affect the shape of the limb profile. *Hinteregger et al.* [1981] developed reference solar spectra based on rocket measurements and obtained extreme ultraviolet (EUV) irradiances using the Atmospheric Explorer (AE)-C and AE-E spectrometers. To quantify the solar soft X-rays and EUV irradiance on a particular day, numerous studies have adopted the *Hinteregger et al.* [1981] results. However, solar EUV emissions vary by a factor of two over the solar cycle and some portions of the X-ray spectrum may vary by more than an order of magnitude [*Solomon and Qian*, 2005]. Observations from 1998 to 1999 by the Student Nitric Oxide Explorer (SNOE) indicate the Hinteregger algorithm significantly underestimates the emissions in the 20–200 Å region [*Solomon et al.*, 2001].

[7] The third of the factors examined is the influence of photoabsorption by O_2. Emissions from the LBH bands are attenuated by O_2 photoabsorption, especially at the lower altitudes, in the O_2 Schumann-Runge (S-R) continuum, which occurs in the same wavelength range as the N_2 LBH bands. Measurements of the O_2 photoabsorption cross section within the S-R continuum indicate that the cross section increases with temperature; however, atmospheric temperatures near the peak of the LBH emission are substantially higher than have been used in recent laboratory measurements. An even more significant source of uncertainty in the amount of absorption by O_2 is the uncertainties in the atmospheric O_2 density. But, basing the neutral densities on satellite drag data, as will be done here, decreases this source of uncertainty.

[8] In order to better understand the possible effects of the three factors considered, model-to-model and observations-to-model comparisons are examined in the following sections. The Global Airglow (GLOW) model is used to calculate the direct excitation by photoelectron impact and the Intrasystem Cascade Excitation (ICE) model is used to calculate the expected contribution from cascading and Collision Induced Electronic Transitions (CIET) [*Eastes*, 2000]. The observations were made by the High resolution Ionospheric and Thermospheric Spectrograph (HITS) aboard the Advanced Research and Global Observation Satellite (ARGOS).

2. Observations

[9] This section describes the HITS observations used for comparisons with the calculated limb profiles, as well as the satellite drag data used to constrain the neutral atmosphere used in the modeling calculations.

2.1. ARGOS/HITS Data

[10] The ARGOS satellite was launched on 23 February 1999 into a sun-synchronous orbit at an altitude of 840 km. This orbit crossed the dayside equator at ~1430 Local Time. ARGOS began operations on 15 May 1999. HITS observed in 110 Å passbands between 500 and 1800 Å with a spectral resolution of ~1.3 Å full width at half maximum (FWHM) [*Dymond et al.*, 1999]. While HITS provides high spectral resolution, the photometric sensitivity is low; consequently, significant amounts of data, approximately 1 day, are summed together for this study.

[11] The observations used in this study were obtained while HITS scanned the limb on the Earth's dayside with an integration period of one second per spectral scan. In each limb scan there are approximately 120 spectra. Limb scans for which the solar zenith angle (SZA) at the tangent point was less than 50° are selected for analysis. Due to a "warm spot" on the microchannel plate (MCP) detector, noise occasionally increased for ~15 s in the area where the shortest wavelength emissions were observed. Spectra exhibiting this localized MCP noise are identified by comparisons between the emissions within each spectrum, with adjacent spectral scans and with the expected SZA variation of the emissions and omitted from the sums used in the

Table 1. The Number of Individual Spectra Averaged to Measure LBH (1,1) Band Brightness

Average Tangent Altitude (km)	Number of Spectra Summed		
	28 July 2001	29 July 2001	30 July 2001
105	405	437	345
120	417	476	362
135	356	370	301
145	209	233	182
150	134	145	116
155	142	154	122
160	133	156	120
165	145	166	122
170	213	246	189
180	454	525	393
200	603	677	513
220	616	686	499
240	669	752	543
260	655	715	544
180	677	732	565
300	705	761	599
320	691	735	588

analysis. Spectra with noise from the South Atlantic Anomaly are easily identified by strong uniform noise across the detector and the by geographical location of *ARGOS*, and likewise excluded. The remaining observations, equivalent to approximately 60 full limb profiles, are used to produce an average limb profile for each day. Due to the SZA restrictions and the satellite orbit, the observations are almost evenly distributed across geographic latitudes of approximately −10° to 64°. The average latitude for the observations used on each of the three days is ~26°. Both the filtering of the data described earlier and the higher latitude limit help exclude auroral contributions, as does the filtering performed after the spectra are binned by tangent altitude. In each altitude bin, any spectrum for which the brightness in the LBH (1,1) band deviates from the average by more than three sigma is excluded. The resulting number of spectra as a function of tangent altitude and the central altitude of each bin is listed in Table 1 for the days analyzed (28–30 July 2001).

[12] The 1440–1550 Å, passband, which is used in this paper and shown in Figure 1, includes emissions from vibrational levels 0–6. The (1,1) band at 1464 Å, gives the largest signal-to-noise ratio of the bands observed. Although the instrument response across the 1440–1550 Å passband is estimated to vary by approximately 20% [*Dymond et al.*, 1999], this variation should not affect the results in this paper because the analysis depends on the relative brightness of only the (1,1) band as a function of tangent altitude. While an absolute calibration is desirable, it is not necessary for determining the agreement between the shapes (variation with altitude) of the observed and modeled emission profiles. The accuracy of temperatures retrieved from either the scale heights or the rotational temperatures of the LBH bands depends on an accurate understanding of the factors that determine the shape of the profile, even for observations near nadir, as when observing Earth from a geostationary orbit. However, observational information about the shape of the profile is only available when limb viewing.

[13] To derive the (1,1) band brightness profile on each of the three days, a nonlinear least squares approach is used to fit synthetic spectra to those observed at each tangent altitude. This fitting uses discrete inverse theory (DIT) [*Menke*, 1989] to find the contributions, by both the (1,1) band and the background, that produce the best fit to the observed spectra. A Levenberg-Marquardt (LM) [*Marquardt*, 1963] scheme is used to adjust the parameters and minimize chi-square values. For more details, see *Aksnes et al.* [2006, 2007]. The fitting used in this analysis differs from that described by *Aksnes et al.* [2006, 2007] only in that (1) atmospheric temperature variations along the line of sight are included during the fitting (by using a Mass Spectrometer and Incoherent Scatter (MSIS) model profile whose exospheric temperature matches that derived from the coincident satellite drag measurements discussed in section 2.2) and (2) the wavelength shift used for all the spectra is an average of the shifts derived from the individual spectra observed below 200 km tangent altitude. Since altitude-dependent or day-dependent differences in the wavelength shift were not discernable (as expected, since the grating position was unchanged during the three days of observations), an average wavelength shift was used when deriving all the (1,1) band brightnesses.

2.2. Satellite Drag Data

[14] Satellite drag data are one of the most reliable sources of data for characterizing thermospheric density. For each day of the HITS observations, drag data from 11 satellites was used to select the F10.7 values that provided the best agreement between densities from the MSIS 2000 model and those derived from the drag measurements. The data used are a subset of those used by *Bowman et al.* [2008] to update their empirical model of the neutral densities. Daily and average (81 day) values of F10.7 were set equal during the selection. The satellites used for the analysis had perigee

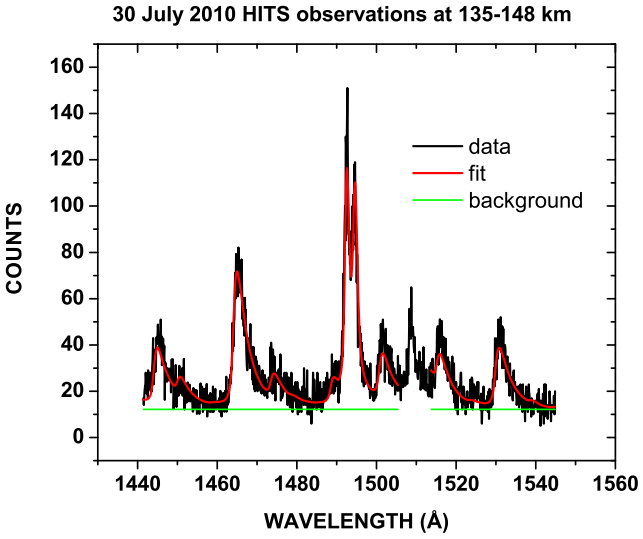

Figure 1. The average HITS spectrum (black) and the best fit synthetic spectrum (red) obtained on 30 July 2001 at tangent altitudes of 140–150 km. In order to accurately establish a background (green), the initial fitting of the spectrum incorporates LBH emissions from v = 0–6 and the atomic nitrogen doublet at 1493 Å. The LBH (4,4) emission around 1509 Å has been omitted due to uncertainties in the detector response.

altitudes of 405 km or less (220–405 km), and their perigees were almost uniformly distributed at latitudes below 70° except for one satellite with a perigee near 80°. For 28, 29, and 30 July, the derived values of F10.7 were 140.5 ± 6.2, 137.6 ± 4.9 and 137.2 ± 5.5, respectively.

3. Modeling of the LBH Emission Profile

[15] Model calculations are used for both the model-to-model and observations-to-model comparisons. This section describes the modeling parameters used in the comparisons.

[16] For the model-to-model comparisons, two input parameters are varied when modeling the LBH emission profiles: the solar irradiance spectrum and the O_2 photoabsorption cross section. In addition all the calculations are performed with and without excitation of the LBH bands by cascade from other singlet states. Since there are uncertainties in the cascade calculation, the calculations without cascade allow its role to be more clearly understood. Volume emission rates from the models are calculated on ~1/6 scale height grid, in altitude, except for altitudes near the emission peak, 150–160 km, where a 1 km grid is used. From these volume emission rates, line-of-sight (LOS) brightnesses are calculated for a uniform angular grid, since the HITS instrument scanned the limb at a uniform angular rate. The altitude spacing, 0.5–1.8 km, in this angular grid is ~1.6 km near 150 km and increased at the lower altitudes. From these LOS brightnesses, values are interpolated onto a uniform 1 km altitude grid for comparisons. In the model, daily and average F10.7 are both set to 140, approximately the value derived from the satellite drag data during the HITS observations, as discussed in section 2, and Ap is set to 4.0, approximately the value recorded for 28–30 July.

[17] For the observations-to-model comparisons, the same approach as above is used (varying the solar spectrum, etc.), but the line-of-sight brightnesses are binned, in altitude, using the algorithm that is used for the observations. Also, the F10.7 values derived from the satellite drag data and the observed Ap are used in the model calculations. Using these values, profiles are calculated on a 5° latitude by 60° longitude grid for −10° to +65° latitude and 0° to 300° longitude. The average of these profiles at the LBH (1,1) band, at 1464 Å, is calculated for comparison with the observed profile.

3.1. Solar Spectrum and Irradiance

[18] Both the total solar irradiance and the spectral distribution (irradiance as a function of wavelength) of the solar spectrum affect the calculated emission profile. Since the HITS observations occurred during a period when solar irradiance measurements from neither the SNOE satellite nor the TIMED satellite are available, model calculations of the solar spectrum are used, and the analysis concentrates on the effects of the spectrum's shape.

[19] Four different solar irradiance spectra are used for calculating the LBH emissions. Three of the four spectra use Hinteregger's algorithm with the irradiances at wavelengths of 17–250 Å scaled by 1, 2, or 3. A scaling factor of ~3 has often been used when calculating atmospheric, ultraviolet emissions. In the fourth spectrum, scaling factors of 6, 4, and 5 - which will be referred to as the *Solomon et al.* [2001] scaling - are applied to Hinteregger's algorithm in the 17–70 Å, 70–170 Å, and 170–200 Å wavelength ranges, respectively, as suggested by *Solomon et al.* [2001] and S. Bailey (personal communication, 2006). These scaling factors are based on analysis of solar data from SNOE. Although the *Solomon et al.* [2001] scaling factors are larger, they give essentially the same airglow brightness as the factor of 3 scaling which is applied to a slightly broader (17–250 Å versus 17–200 Å) wavelength range. However, the Solomon scaling increases the irradiance at the shorter wavelengths of the solar spectrum, which increases the emission at the lower altitudes, as will be shown below.

3.2. O_2 Photoabsorption

[20] The modeled brightness as a function of tangent altitude is obtained by line-of-sight integration of the volume emission rates while including attenuation by O_2 photoabsorption. Errors in the amount of photoabsorption could result from errors in either the O_2 column density or the photoabsorption cross section. Both possibilities have similar effects on the observed emission. Therefore, in the comparisons with observations, scaling of the O_2 density is used to account for this possible source of error, while the photoabsorption cross section is scaled in the model-to-model comparisons.

[21] Using satellite drag data to constrain the densities used in the calculation should decrease the density errors. For comparisons between observations and models for the three geomagnetically calm days, three separate model calculations for each day are used. In addition to the model calculations with the F10.7 derived from the drag data, calculations for F10.7 ± 1 σ values are included. When using the MSIS 2000 model, the uncertainties in F10.7 correspond to uncertainties of ~1 part in 100 or less in the total O_2 column density for emissions from altitudes below 180 km, where the effects of photoabsorption are most significant.

[22] The O_2 photoabsorption cross section varies with temperature, and few of the available measurements cover the range of temperatures seen in the Earth's thermosphere. Errors in the cross section are expected to be small at the temperatures that have been well measured, below ~575K. However, those measurements [e.g., *Kanik et al.*, 1997; *Yoshino et al.*, 2005] indicate the O_2 cross section increases with temperature, and much of the Earth's LBH emission comes from altitudes where the temperature is higher, ~750 K. Given the large range of temperatures expected, ~170 K at 112 km to ~1000 K at 300 km, in the atmosphere being observed, a temperature dependence as well as scaling of the O_2 density was used in the data-to-model comparisons, but for the model-to-model comparisons, the calculations were simplified by using three fixed cross sections.

3.3. Excitation Processes

[23] Limb profiles of the LBH emissions are modeled with and without cascading between the singlet electronic N_2 states. The former is performed by using ICE [*Eastes and Dentamaro*, 1996] to augment the GLOW model [e.g., *Solomon et al.*, 2001]. This model include excitation from v = 0–2 of the N_2 ground state (assumes the cross sections for those states are the same as for v = 0); radiative and collisional cascade processes between the a and a′

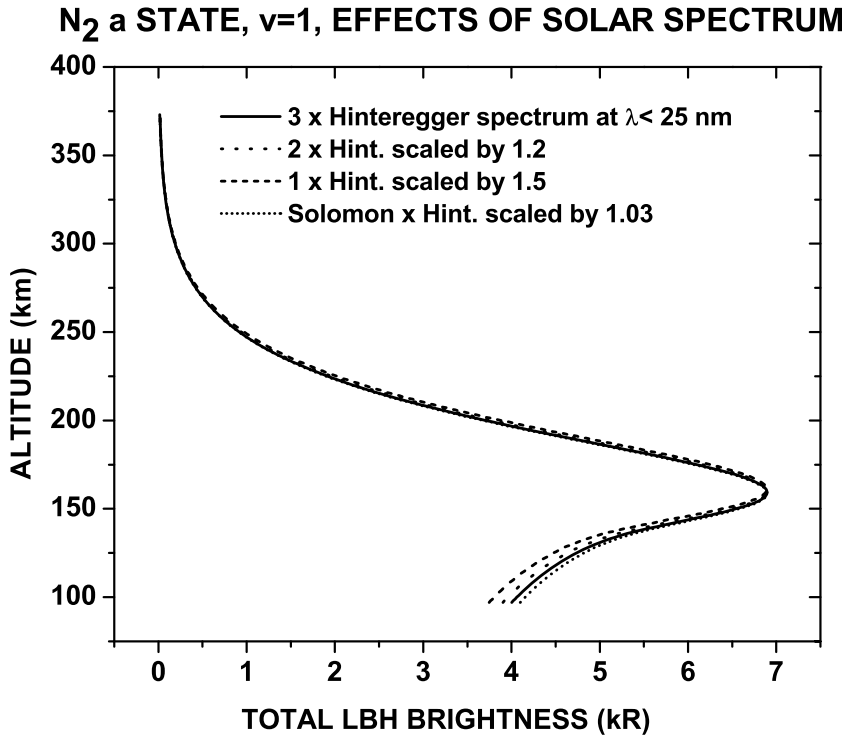

Figure 2. Modeled limb profiles of the LBH, v = 1, emission using solar flux values provided by different scaling (1, 2, and 3) of the Hinteregger solar spectrum, at wavelengths of 25 nm and less, or the *Solomon et al.* [2001] scaling at wavelengths below 20 nm, as discussed in section 1. An O_2 photoabsorption cross section of 1.5×10^{-18} cm^2 and F10.7 (daily and average) of 140 were used. The emission profile from the straight Hinteregger spectrum peaks highest (1–2 km) due to the lower solar flux below 25 nm. The *Solomon et al.* [2001] scaling increases the shorter wavelength emissions from the Sun, resulting in slightly more emission at the lower altitudes.

states and the a and w states; and quenching of the excitation to the a, a′ and w states. Previous modeling of the cascade contributions [*Eastes and Dentamaro*, 1996] used the CSD model [*Jasperse*, 1976], which makes approximations in order to simplify the calculation of the photoelectron spectrum. In addition to changing the photoelectron model, the cross sections by *Young et al.* [2010], the most recent measurements available, were used when calculating the volume emission rates. To obtain a′ and w state excitation rates, the results of *Johnson et al.* [2005], who measured excitation cross sections for all three of the singlet states, were used. The resulting a state cross sections are almost a factor of two smaller than the *Ajello and Shemansky* [1985] cross sections used in the *Eastes* [2000] paper. However, *Young et al.* [2010] did not directly establish an absolute cross section, and the shape of their a state cross section is significantly different that found in previous measurements. Due to the differences in shape, normalizing the *Young et al.* [2010] cross section at 18 eV rather than 100 eV, near the peak rather than in the tail, increases the peak value by a factor of approximately two. Consequently, the calculated brightnesses could be low.

4. Model-to-Model Comparisons

[24] Profiles were calculated for comparing the effects of each of the parameters considered: the O_2 photoabsorption cross section, the solar irradiance spectrum and excitation by cascade. The effect of each parameter on the emission profile is discussed below. Although the brightness of the emission varies substantially, the shape of the profile above the peak and the peak altitude do not change significantly.

4.1. Solar Spectrum and Irradiance Effects

[25] Shown in Figure 2 are the LBH limb profiles calculated for 29 July 2001 when using the four scaling of the solar spectra discussed in section 3. All the solar spectra are based on an F10.7 of 140, and all the profiles have been scaled to the same amplitude in order to better show the relative effects of all four scalings of the solar spectrum. For all the calculations an Ap of 4.0 is used. The photoelectron spectra calculated using either GLOW or AURIC models, two of the most modern available, are similar and an example from the latter is available in the work of *Strickland et al.* [1999]. Although these LBH calculations include cascade, the relative effects of the solar spectrum are essentially identical for calculations without cascade.

[26] The differences in the magnitudes of the profiles (or equivalently, the scaling factors used) is attributed to the scaling used for the solar spectrum. Scaling the shorter wavelengths changes the energy deposited in the atmosphere and consequently the total amount of emission. The shapes of the profiles also follow the expected pattern, because the shorter wavelengths of the solar spectrum, which are being scaled, are the ones that penetrate furthest into the atmosphere. Consequently, increasing the shorter wavelength

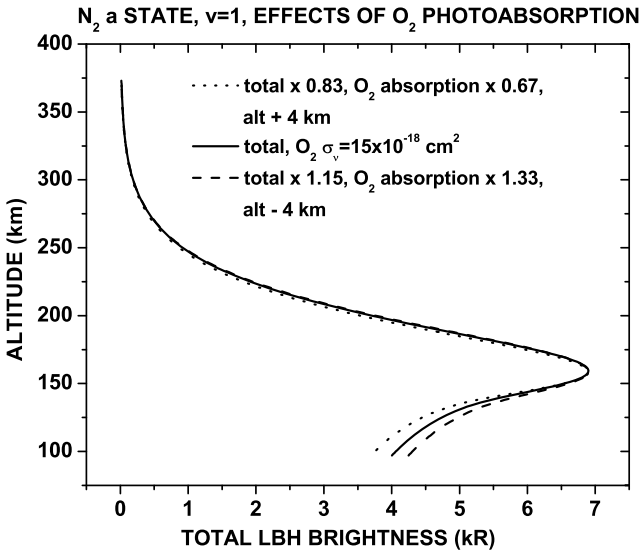

Figure 3. Modeled LBH limb emission profiles calculated using the Hinteregger algorithm with a scaling of 3 and cascading. The peak magnitudes and locations are adjusted to match that calculated when using an O_2 photoabsorption cross section 15×10^{-18} cm^2 (solid line).

solar emissions increases the emissions at the lower altitudes. It is clear that the total emission produced is almost identical when using either the *Solomon et al.* [2001] scaling or the 3× scaling of the Hinteregger spectrum (which has been typically used when modeling the daytime airglow emissions). However, as discussed by *Solomon et al.* [2001], the ionospheric density profiles differ.

[27] There is a small difference between the peak altitudes for the profiles. However, an altitude shift of only 1–2 km is the maximum difference seen between the four solar spectra. Such an altitude difference, which depends on drastic differences in the solar spectrum, corresponds to a change of 6–20 K in the temperature at the peak of the profile, or in the thermospheric temperature that would be derived from the LBH bands.

4.2. O_2 Photoabsorption Effects

[28] The effects of O_2 photoabsorption on the LBH limb profiles is shown in Figure 3. Limb emissions were modeled using cross sections of 10, 15, and 20×10^{-18} cm^2 and using Hinteregger's algorithm with a scaling factor of 3. Since changes in the O_2 cross section and number density have similar effects, changes in the cross section alone are considered. For the (1,1) band of the LBH emission (1464 Å), a photoabsorption cross section of $\sim 15 \times 10^{-18}$ cm^2 would be expected at the temperatures near the peak of the emission profile. In Figure 3 the modeled limb profiles are scaled to the same amplitude and shifted to the same peak altitude. Decreasing the photoabsorption cross section to 10×10^{-18} cm^2 (decreasing the O_2 photoabsorption by a factor of 0.67), causes the total emission to increase (by a factor of 1/0.83) and peak ~4 km lower in altitude. Conversely, increasing the cross section decreases the total emission (by 1/1.15) and increases the peak altitude calculated by ~4 km. After the peaks are aligned and scaled to the same magnitude, one can see that there are only slight differences in the shape of the profile at the higher altitudes, but appreciable differences appear at the lower altitudes. When nadir viewing the result is less sensitive to changes in photoabsorption by O_2. Decreasing the photoabsorption cross section from 15×10^{-18} cm^2 to 10×10^{-18} cm^2 results in the contribution peaking ~1 km lower, where the thermospheric temperature would be ~10 K lower.

4.3. Excitation Process Effects

[29] In Figure 4, modeled emissions calculated using GLOW only (i.e., direct excitation only, dotted line) and GLOW + ICE (i.e., direct plus cascade, solid line) are shown. Cascading increases the v = 1 emission by a factor of ~1.4; however, the effects of cascade vary with vibrational level and emissions from the higher vibrational levels are decreased. Consequently, the total LBH emission increases by ~1.1. This increase in emission, due to the addition of excitation by cascade, is less than reported previously (~1.6) by *Eastes* [2000] for two reasons. The first is that the a′ and w state excitation is less, relative to the a state, when using the *Johnson et al.* [2005] cross sections rather than those of *Cartwright* [1978] which were used previously. The second, and most important reason, is the exclusion of contributions from a′ and w state vibrational levels which lie above v = 6 of the a state. For the a state, these higher vibrational levels are predissociated. When energy cascade is included in the model, the calculated emissions from vibrational levels above v = 3 of the a state are less than when using direct excitation alone due to the loss of excitation to states other than the ground state of N_2. The calculated contribution from cascade is at the lower end of the range of values reported for

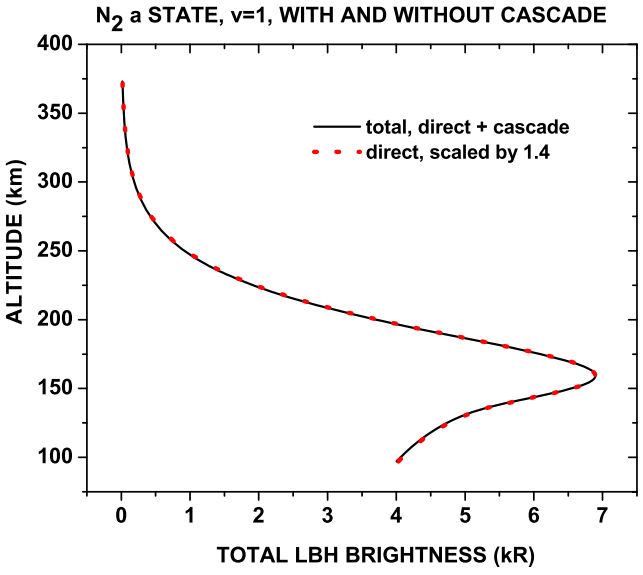

Figure 4. Modeled limb profiles of the LBH, v = 1, emission with (GLOW + ICE, solid line) and without cascade (GLOW alone, dotted line). When cascading is included, the profile is slightly narrower than it is without. The calculations use the Hinteregger solar flux scaled by 3, at wavelengths of 25 nm and less, an O_2 photoabsorption cross section of 1.5×10^{-18} cm^2 and an F10.7 (daily and average) of 140.

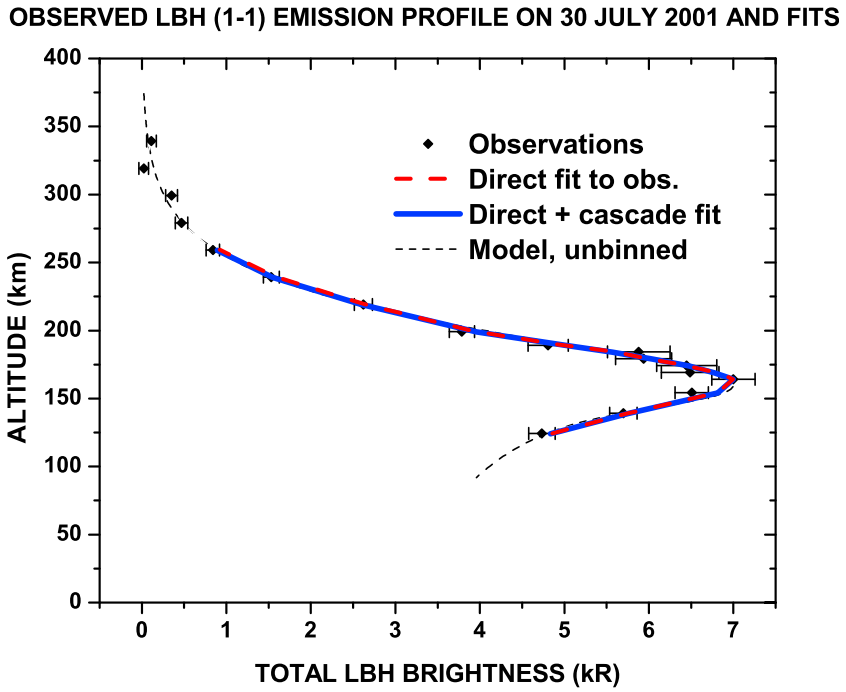

Figure 5. Modeled (solid line) and measured (diamonds, with $\pm 1\sigma$ error bars) LBH (1,1) band N_2 emissions for 30 July 2001. The modeled emission values are calculated using GLOW + ICE, the formula by *Hinteregger et al.* [1981] with scaling = 1, and an O_2 photoabsorption cross section of $\sim 15 \times 10^{-18}$ cm^2. For comparison the measured values have been scaled to match the calculated magnitude of the LBH bands.

the cascade enhancement. Results from the other analyses, summarized by *Ajello et al.* [2011], range from 1.25 to 1.74.

[30] The model results vary significantly, depending on the vibrational level. The modeled emissions of the a state using GLOW alone and GLOW + ICE differ by factors of approximately 1.8–0.9, depending on the vibrational level. These factors increase if excitation from higher lying a′ and w states is included, and the total emission also increases. This dependence of cascade effects on the vibrational level would contribute to the variation in experimental results, which have not used a uniform methodology.

[31] While the total brightness is model dependent, the peak altitude is model independent for most vibrational levels. For nadir viewing, peak altitudes differ by ~1 km for the lowest vibrational levels, which are most affected by cascade, but the calculated shifts are insignificant (≤ the 0.25 km grid spacing used in the calculation) for most vibrational levels (v = 2–6).

5. Observations-to-Model Comparisons

[32] To determine the observations-to-model agreement, limb profiles from three days (28, 29 and 30 July 2001) are compared with model calculations. Limb profiles were calculated for combinations of the three parameters examined earlier, and the peak altitude and magnitude of the resulting profiles were then adjusted to achieve a best fit. The model calculations and the best of these fits are discussed below.

[33] When calculating emission profiles for comparison with the observations, the parameters examined in the model-to-model comparisons were used. However, the temperature dependence of the O_2 cross section was included. Although omitting that dependence is not expected to affect the model-to-model comparisons, since the effect should be similar for both calculated profiles, it will influence the observed profiles. For each of the three days, combinations of parameters were explored to identify the combination that provided the best fit for each day. Three F10.7 values were used for each day, that derived from the drag measurements on that day and the $\pm 1\sigma$ values, as indicated earlier. Two scalings of the Hinteregger solar spectrum, that of Solomon and a factor of three scaling, were used. For each of the six combinations of F10.7 and solar spectrum, the scaling of the O_2 density was varied in increments of 0.1 from the nominal density.

[34] On each of the three days, the combination of parameters producing the lowest chi-square values during the fits with and without cascade are similar. For 28 July 2001, F10.7 = 146.75, O_2 scaling of 0.8, and the Solomon scaling of the solar spectrum produced the best fits, giving a reduced chi-square of 0.61 with cascade and 0.59 without. For 29 July, F10.7 = 142.55, O_2 scaling of 0.7 and the Solomon scaling of the solar spectrum produced the best fits, giving a reduced chi-square of 0.75 with cascade and 0.62 without. The fits from 30 July are the best, giving a reduced chi-square of 0.25 with cascade and 0.30 without. An example of both the observed and calculated altitude profiles for 30 July is shown in Figure 5. As shown in Table 1, the number of spectra used to determine this profile is less than for the other two days. Consequently, since the solar irradiance, and dayglow brightness, are similar for all three days, the uncertainties are largest for the 30 July profile. The low

chi-square values (<1) indicate that the statistical errors for the (1,1) band signal, which are derived by fitting the spectrum and background, are overestimates. This is consistent with comparisons of the errors estimated while fitting synthetic data and the known errors for the synthetic data, but a resolution of this discrepancy is beyond the scope of this analysis.

[35] In Figure 5 the observed emissions (diamonds, with $\pm 1\sigma$ error bars) have been shifted upward in altitude by the ~18.2 km necessary for a best fit between them and the modeled (solid line) LBH emissions. The shifts are similar, within tenths of a km, for fits with or without cascade and show no systematic differences for observations on 28, 29, and 30 July. For the two earlier days, 28 and 29 July, the altitude shifts are 14.3 km and 18.2 km, respectively. These altitude shifts are in excellent agreement with observations of a bright star (HD108073) by both HITS and LORAAS on 29 July. For both instruments the discrepancy, 4–5 s or ~0.34 degrees, between the time the star was observed and the time expected from the pointing data is equivalent to the 18 km discrepancy in tangent altitude. These differences could be explained by either a small error in the pointing information for the spacecraft or a substantial error in the exospheric temperature. Since drag data have been used to quantify the density of the neutral atmosphere, which corresponds to the exospheric temperature, the pointing information is the most likely cause for the difference.

[36] The differences between the fits with and without cascade are small, but the fits using direct excitation alone are better for two of the three days. This difference is due to the direct excitation profile being slightly wider, in altitude, than that produced when cascade is included, and the observed profile being almost imperceptibly broader in altitude than either calculated profile. The profiles from the other two days, 28 and 29 July, are smoother above the peak, while the data for 30 July, shown in Figure 5, contain a point, just above the peak, which has a larger than typical brightness relative to the adjacent measurements. That point, in effect, makes the 30 July profile peak more sharply than those for 28 and 29 July. It is clear that the differences between the observed and either of the calculated profiles is greater than the differences between the calculated profiles.

[37] There are at least three potential reasons for direct excitation alone generally fitting better: (1) direct excitation alone is responsible for the LBH emission; (2) the actual temperature-density profile of the lower thermosphere differs from the empirical MSIS 2000 model used in the analysis; and (3) there is an error in the background signals subtracted. While the first explanation cannot be eliminated using these observations, it does not appear to be consistent with laboratory measurements of electron excitation cross sections, reaction rates and lifetimes of the singlet states of molecular nitrogen. The second possibility, a discrepancy between the modeled and actual profiles, is consistent with the effects of energy from waves and tides being deposited in the lower thermosphere. The altitude profile in the MSIS model does not include energy input from below. When upward propagating waves from the lower atmosphere break due to the atmospheric density decreasing, most of their energy is deposited in the lower thermosphere, increasing the temperature there. The associated density changes would be expected to decrease the rate at which density decreases with altitude and produce a flatter emission profile. The third possibility cannot be eliminated. Although extensive efforts were made to avoid errors in the background removed, the LBH emission decreases much more rapidly with altitude than the background does. Consequently, if the backgrounds are low, then the LBH emission would appear to decrease more slowly with altitude. A fourth possibility, mechanical wear on the scan mechanism, was considered but dismissed because such wear would not alter the optical encoder readings from which the angular position information is derived.

6. Conclusions

[38] Comparisons of the shapes of limb profiles from satellite observations and model calculations of the N_2 LBH emissions consistently show excellent agreement, indicating that the current models of the atmospheric emission profile are suitable for deriving thermospheric temperatures from remote sensing measurements of the LBH bands. While slightly better results are obtained from calculations without cascading between the singlet states for two of the three days examined, the observed profiles are in good agreement with either of those calculated. Although the differences for individual days are negligible, the presence of similar differences suggests that an additional mechanism could have a minor influence on the shape. At least three possible sources for the small differences between the observed and either of the calculated profiles are identifiable, but these analyses could not distinguish between them. Only one of those three, heating of the lower thermosphere by upward propagating waves and tides, would be associated with an actual change in the emission profile.

[39] The model results presented here also suggest there may be less enhancement of the LBH band emissions (from cascade) than do the results previously presented by *Cartwright* [1978], *Eastes and Dentamaro* [1996], and *Eastes* [2000]. Changes in the excitation cross sections contribute to the difference, but most of the difference is due to the assumption that states above the v = 6 predissociation threshold for the a state do not contribute to the excitation available to the a state. These new calculations of the LBH brightness suggest that the enhancement expected from cascade may vary by a factor of two, depending on the vibrational level, and is largest for the lowest levels of the a state.

[40] **Acknowledgments.** The effort at the University of Central Florida was supported by NASA grants NNG06GI94G and NAG5-12786 and by NSF grant 0850396. The effort at NRL was supported by NRL Base Program work unit 76–9880. The authors gratefully acknowledge Frank Marcos for providing the satellite drag data used in the analysis. In addition, Arun Kulshreshth is acknowledged for combining the GLOW and ICE codes.

[41] Robert Lysak thanks the reviewers for their assistance in evaluating this paper.

References

Ajello, J. M., and D. E. Shemansky (1985), A reexamination of important N_2 cross sections by electron impact with application to the dayglow: The Lyman-Birge-Hopfield band system and N I (119.99 nm), *J. Geophys. Res.*, *90*, 9845–9861, doi:10.1029/JA090iA10p09845.

Ajello, J. M., R. S. Mangina, and R. R. Meier (2011), UV molecular spectroscopy from electron impact for applications to planetary atmospheres and astrophysics, in *Charged Particle and Photon Interactions With*

Matter: Recent Advances, Applications, and Interfaces, edited by Y. Hatano et al., pp. 761–804, CRC Press, Boca Raton, Fla.

Aksnes, A., R. Eastes, S. Budzien, and K. Dymond (2006), Neutral temperatures in the lower thermosphere from N_2 Lyman-Birge-Hopfield (LBH) band profiles, *Geophys. Res. Lett.*, *33*, L15103, doi:10.1029/2006GL026255.

Aksnes, A., R. Eastes, S. Budzien, and K. Dymond (2007), Dependence of neutral temperatures in the lower thermosphere on geomagnetic activity, *J. Geophys. Res.*, *112*, A06302, doi:10.1029/2006JA012214.

Bowman, B. R., W. K. Tobiska, F. A. Marcos, C. Y. Huang, C. S. Lin, and W. J. Burke (2008), A new empirical thermospheric density model JB2008 using new solar and geomagnetic indices, *Pap. 2008–6438*, Am. Inst. of Aeronaut. and Astronaut., New York.

Budzien, S. A., P. D. Feldman, and R. R. Conway (1994), Observations of the far ultraviolet airglow by the Ultraviolet Limb Imaging experiment on STS-39, *J. Geophys. Res.*, *99*, 23,275–23,287, doi:10.1029/94JA01543.

Cartwright, D. C. (1978), Vibrational populations of excited states of N_2 under auroral conditions, *J. Geophys. Res.*, *83*, 517–531, doi:10.1029/JA083iA02p00517.

Christensen, A. B., et al. (2003), Initial observations with the Global Ultraviolet Imager (GUVI) in the NASA TIMED satellite mission, *J. Geophys. Res.*, *108*(A12), 1451, doi:10.1029/2003JA009918.

Dymond, K. F., K. D. Wolfrom, S. A. Budzien, C. B. Fortna, and R. P. McCoy (1999), High-resolution ionospheric and thermospheric spectrograph (HITS) on the Advanced Research and Global Observation Satellite (ARGOS): Quick look results, *Proc. SPIE Int. Soc. Opt. Eng.*, *3818*, 137–145, doi:10.1117/12.364149.

Eastes, R. W. (2000), Modeling the N_2 Lyman-Birge-Hopfield band in the dayglow: Including radiative and collisional cascading between the singlet states, *J. Geophys. Res.*, *105*, 18,557–18,573, doi:10.1029/1999JA000378.

Eastes, R. W., and A. V. Dentamaro (1996), Collision-induced transitions between the $a^1\Pi_g$, $a'^1\Sigma^-_u$, and $w^1\Delta_u$ states of N_2: Can they affect auroral N_2 Lyman-Birge-Hopfield band emissions?, *J. Geophys. Res.*, *101*, 26,931–26,940, doi:10.1029/96JA01636.

Eastes, R. W., and W. E. Sharp (1987), Rocket-borne spectroscopic measurements in the ultraviolet aurora: The Lyman-Birge-Hopfield bands, *J. Geophys. Res.*, *92*, 10,095–10,100, doi:10.1029/JA092iA09p10095.

Eastes, R. W., P. D. Feldman, E. P. Gentieu, and A. B. Christensen (1985), The ultraviolet dayglow at solar maximum: 1. Far UV spectroscopy at 3.5 Å resolution, *J. Geophys. Res.*, *90*, 6594–6600, doi:10.1029/JA090iA07p06594.

Eastes, R. W., et al. (2008), Global-scale Observations of the Limb and Disk (GOLD): New observing capabilities for the ionosphere-thermosphere, in *Midlatitude Ionospheric Dynamics and Disturbances*, *Geophys. Monogr. Ser.*, vol. 181, edited by P. M. Kintner Jr. et al., pp. 319–326, AGU, Washington, D. C., doi:10.1029/181GM29.

Hinteregger, H. E., K. Fukui, and B. R. Gilson (1981), Observational, reference, and model data on solar EUV, from measurements on AE-E, *Geophys. Res. Lett.*, *8*, 1147–1150, doi:10.1029/GL008i011p01147.

Jasperse, J. R. (1976), Boltzmann-Fokker-Planck model for the electron distribution function in the Earth's ionosphere, *Planet. Space Sci.*, *24*, 33–40, doi:10.1016/0032-0633(76)90058-1.

Johnson, P. V., C. P. Malone, I. Kanik, K. Tran, and M. A. Khakoo (2005), Integral cross sections for the direct excitation of the A $^3\Sigma^+_u$, B $^3\Pi_g$, W $^3\Delta_u$, B′ $^3\Sigma^-_u$, a′ $^1\Sigma^-_u$, a $^1\Pi_g$, w $^1\Delta_u$, and C $^3\Pi_u$ electronic states in N_2 by electron impact, *J. Geophys. Res.*, *110*, A11311, doi:10.1029/2005JA011295.

Kanik, I., L. Beegle, C. Noren, S. M. Ahmed, and R. Link (1997), Temperature-dependent photoabsorption cross section measurements of O_2 at the NI airglow and auroral emission lines, *Chem. Phys. Lett.*, *279*, 297–302, doi:10.1016/S0009-2614(97)01077-4.

Marquardt, D. W. (1963), An algorithm for least-squares estimation of nonlinear parameters, *J. Soc. Ind. Appl. Math.*, *11*, 431–441, doi:10.1137/0111030.

Meier, R. R. (1991), Ultraviolet spectroscopy and remote sensing of the upper atmosphere, *Space Sci. Rev.*, *58*, 1–185, doi:10.1007/BF01206000.

Meier, R. R., G. Crowley, D. J. Strickland, A. B. Christensen, L. J. Paxton, D. Morrison, and C. L. Hackert (2005), First look at the 20 November 2003 superstorm with TIMED/GUVI: Comparisons with a thermospheric global circulation model, *J. Geophys. Res.*, *110*, A09S41, doi:10.1029/2004JA010990.

Menke, W. (1989), Geophysical Data Analysis: Discrete Inverse Theory, Int. Geophys. Ser., vol. 45, Academic, San Diego, Calif.

Solomon, S. C., and L. Qian (2005), Solar extreme-ultraviolet irradiance from general circulation models, *J. Geophys. Res.*, *110*, A10306, doi:10.1029/2005JA011160.

Solomon, S. C., S. Baily, and T. Woods (2001), Effect of solar soft X-rays on the lower ionosphere, *Geophys. Res. Lett.*, *28*, 2149–2152, doi:10.1029/2001GL012866.

Strickland, D. J., J. Bishop, J. S. Evans, T. Majeed, P. M. Shen, R. J. Cox, R. Link, and R. E. Huffman (1999), Atmospheric ultraviolet radiance integrated code (AURIC): Theory, software architecture, inputs, and selected results, *J. Quant. Spectrosc. Radiat. Transfer*, *62*, 689–742, doi:10.1016/S0022-4073(98)00098-3.

Strickland, D. J., R. R. Meier, R. L. Walterscheid, A. B. Christensen, L. J. Paxton, D. Morrison, J. D. Craven, and G. Crowley (2004), Quiet-time seasonal behavior of the thermosphere seen in the far ultraviolet dayglow, *J. Geophys. Res.*, *109*, A01302, doi:10.1029/2003JA010220.

Torr, M. R., et al. (1995), A far ultraviolet imager for the International Solar-Terrestrial Physics Mission, *Space Sci. Rev.*, *71*, 329–383, doi:10.1007/BF00751335.

Yoshino, K., W. H. Parkinson, K. Ito, and T. Matsui (2005), Absolute aborption cross-section measurements of Schumann–Runge continuum of O_2 at 90 and 295 K, *J. Mol. Spectrosc.*, *229*, 238–243, doi:10.1016/j.jms.2004.08.020.

Young, J. A., C. P. Malone, P. V. Johnson, J. M. Ajello, X. Liu, and I. Kanik (2010), Lyman–Birge–Hopfield emissions from electron-impact excited N_2, *J. Phys. B At. Mol. Opt. Phys.*, *43*, 135201, doi:10.1088/0953-4075/43/13/135201.

Zhang, Y., L. J. Paxton, D. Morrison, B. Wolven, H. Kil, C.-I. Meng, S. B. Mende, and T. J. Immel (2004), O/N_2 changes during 1–4 October 2002 storms: IMAGE SI-13 and TIMED//GUVI observations, *J. Geophys. Res.*, *109*, A10308, doi:10.1029/2004JA010441.

A. Aksnes, Faculty of Mathematics and Natural Sciences, University of Bergen, N-5020 Bergen, Norway.

S. A. Budzien, Naval Research Laboratory, Code 7607, Washington, DC 20375-5352, USA.

R. E. Daniell, Ionospheric Physics Consulting, 28 Sandy Ridge Rd., Stoughton, MA 02072, USA.

R. W. Eastes and A. Krywonos, Florida Space Institute, Bldg. M6-306, Kennedy Space Center, FL 32899, USA. (richard.eastes@ucf.edu)

D. J. Murray, Department of Physics, University of Central Florida, Orlando, FL 32816, USA.